Published August 29, 2019

Special Section: Nonuniform Flow across Vadose Zone Scales

Core Ideas

- Breakthrough of Br is substantially delayed with respect to the wetting front.
- Film thickness and specific contact area of infiltrating water are calculated.
- Viscous flow approach is successful in both undisturbed and repacked soil columns.
- "Pushing out old water" already occurs at the scale of soil columns.

Viscous Flow Approach to "Pushing Out Old Water" from Undisturbed and Repacked Soil Columns

Christina Bogner* and Peter Germann

The application of bromide tracer in transient infiltration–drainage experiments on undisturbed and repacked soil columns revealed distinct delays of tracer front arrivals with respect to the wetting front arrivals. A viscous flow approach was matched to the flow data that resulted in the parameters film thickness F and specific contact area L of the mobile water with the stagnant parts of the porous medium. Various combinations of F and L were related to the tracer delays, where the combinations $L \times F$, $L \times F^3$, and $L \times F^2$ increasingly showed the highest correlation. The volume of mobile water was turned over 3.8 to 29.5 times between the arrivals of the wetting fronts and the arrivals of the tracer fronts. The delays and their statistical interpretations in view of the viscous flow approach are considered a significant contribution to the understanding of the phenomenon of "pushing out old water" that is still obscured in the hydrology of hillslopes and catchments. Despite the lack of a satisfying explanation for the high numbers of mobile-water turnovers, the fact that the phenomenon of "pushing out old water" already occurs in soil columns may stimulate its investigation at the soil profile scale.

Abbreviations: AWI, air–water interface; BB, Brilliant Blue; LOESS, locally weighted regression; MSE, mean squared error; POOW, pushing out old water; RF, random forests; SWI, solid–water interface; VF, viscous flow; WCW, water content wave.

"Pushing out old water" (POOW) is a well-known phenomenon in the hydrology of hillslopes and first-order catchments. Kirchner (2003), for instance, reports that "in many small catchments, streamflow responds promptly to rainfall inputs, but fluctuations in passive tracers [...] are often strongly damped. This indicates that storm flow in these catchments is mostly 'old' water." The qualifier "old" is a synonym to stored pre-event water and does not refer to its literal age. Kirchner then presents two research questions that, in our opinion, still remain unanswered: "how do these catchments store water for weeks or months, but then release it in minutes or hours in response to rainfall inputs?" and "[...] vary its chemistry according to the flow regime?". For example, Tetzlaff et al. (2014) investigated storage dynamics in hydropedological units in the Scottish upland catchment of Bruntland Burn, using natural ^{2}H and ^{18}O tracers. They identified >80% of the catchment's runoff as "old" water. They also recognized the hydraulic connectivity within the soil catena from the steeper uphill to the intermediate profiles, and down to the valley bottom as a major cause for "old" water to spill into the creek. In contrast, von Freyberg et al. (2018), using the same kind of isotopes, found comparable fractions of "old" water in 24 rainfall–runoff events in the Swiss catchment of Erlenbach. However, in their investigations they favored the routing of pre-event (i.e., "old") and event water as volume fractions of precipitation rather than of discharge. Thus, investigations on POOW in the Scottish catchment are inclined toward the spatial distribution of water storages and their hydraulic connectivity, whereas the analyses in the Swiss catchment stress input routing and residence times. In view of the two contrasting approaches to POOW, Kirchner's (2003) "double paradox in catchment hydrology and geochemistry" still seems unresolved.

Soil hydrology treats solute transport, including tracer transport, primarily with convective–diffusive approaches. Due to diffusion, some of the tracer presumably runs

C. Bogner, Ecosystem Research Group, Institute of Geography, Univ. of Cologne, Zülpicher Straße 45, 50674 Cologne, Germany, and Ecological Modelling, BayCEER, Univ. of Bayreuth, Dr.-Hans-Frisch-Str. 1–3, 95448 Bayreuth, Germany; P. Germann, retired, Univ. of Bern, Switzerland. *Corresponding author (christina.bogner@uni-koeln.de).

Received 13 Sept. 2018.
Accepted 7 May 2019.
Supplemental material online.

Citation: Bogner, C., and G. Germann. Viscous flow approach to "pushing out old water" from undisturbed and repacked soil columns. Vadose Zone J. 18:180168. doi:10.2136/vzj2018.09.0168

ahead of flow and some behind, whereas conservative tracers do not exchange with the porous medium. Quantitative studies on fast preferential flow are gaining ground (e.g., Gerke et al., 2010; Jarvis et al., 2016). They deal primarily with fast flow processes, mainly in relations with assumed soil macropores. However, most of the studies are hardly suited for the investigation of POOW because they ignore equally fast to even faster tracer exchanges that are required to improve our understanding of hydromechanical POOW phenomena. Moreover, convective–diffusive approaches and, more generally, time series of tracer breakthrough are preferably applied to the experimental characterization of preferential flow (Jarvis et al., 2016). Thus, this track of fast flow investigation excludes itself from POOW research. However, viscous flow (VF) parametrization of preferential flow that independently interprets tracer experiments on soil columns offer a novel opportunity for POOW investigations at the small spatial scale of soil columns and soil profiles. In this study, we use such tracer experiments reported by Bogner (2009) to investigate the observed substantial delay of tracer breakthrough with respect to first drainage that we attribute to POOW. Bogner's (2009) experiments were also designed to investigate the presumed difference of infiltration and drainage between columns of undisturbed and repacked soils.

Here, we apply a VF approach (Germann and Karlen, 2016; Germann, 2018a) to the characterization of rapid infiltration and drainage from four columns. Concepts that are based on VF theory are gradually gaining ground in soil hydrology. Nimmo's (2010) source-responsive approach to preferential flow is so far the closest to our VF approach. However, his approach has not evolved to directly deal with the exchange between the mobile and the sessile parts of permeable media, as we propose here. Moreover, Jarvis et al. (2016), on the one hand, deny the validity of Poiseuille-type flow (i.e., VF) to handle preferential flow. On the other hand, Beven (2018), while summarizing the evolution of preferential flow approaches, marks VF favorably among the various types of preferential flow approaches. Further, Atallah and Abou Najm (2019) apply the concept of viscous shear flow to liquids with contrasting viscosities for the experimental determination of pore size distributions in porous media.

Viscous flow describes the water flow in soil as a film with thickness F and a specific contact area L. These VF parameters quantify medium- and process-specific infiltration and drainage. The VF approach assumes that momentum dissipates onto L. Further, we hypothesize that the specific contact area L simultaneously represents the specific surface area available for rapid tracer exchange between the mobile water of VF and the stagnant parts of a porous medium. The VF approach is briefly introduced, and relationships of combined VF parameters vs. delay of tracer breakthrough are explored statistically. Moreover, the comparison of the performances of undisturbed vs. repacked soil columns illustrates the nature of presumed macropores, whereas the suction applied to the column bottoms in the majority of the experiments sheds light on VF.

Material and Methods

Tracer Experiments

Two undisturbed soil columns were extracted from a forest soil (a Norway spruce [*Picea abies* (L.) Karst.] in southeast Germany, 50°08′32.8′′ N 11°51′52.9′′ E). The diameter and height of the soil cores equaled 15 and ∼30 cm, respectively. Additionally, loose soil material was sampled in the vicinity, sieved (<5 mm), and used to pack two columns of the same size and with the same bulk density as the undisturbed ones. The soil properties are given in Supplemental Tables S1 and S2.

Prior to tracer experiments, the columns were saturated from below and subsequently drained to field capacity. Each soil column was irrigated four times with three different irrigation rates, namely 10, 32, and 64 mm h^{-1} (Supplemental Table S3). During the first three irrigation experiments with 10, 32, and 64 mm h^{-1}, respectively, a suction of −10 hPa was applied at the bottom of the soil columns to ensure that the irrigation solution drains directly without saturation (Fig. 1). To trace the breakthrough, Br was added to the irrigation water. The last irrigation experiment on each column was run under atmospheric pressure with 64 mm h^{-1}, whereas the water was ^{18}O-enriched and contained Br, iodide, and Brilliant Blue (BB). The results on iodide and BB are not discussed here.

During a tracer experiment, the weight of the column was monitored every second and the drainage flow was pumped to an autosampler. The sampling rate of the drainage solution depended on the irrigation rate and ranged between 1 and 6 min around the breakthrough of the tracer. Cumulative weight of drainage flow was monitored separately but logged simultaneously to the column weights. In experiments where Br was the only tracer, the columns were irrigated until a constant Br concentration was reached in the drain. When Br, BB, and ^{18}O tracers were combined, irrigation was stopped on the first appearance of BB in the drain.

Bromide concentration in the drainage solution in experiments with Br only was determined with a Br ion-selective electrode (WTW) by adding to 100 mL of drainage solution 2 mL of a 5 M $NaNO_3$ buffer solution. The electrode was calibrated before measurements and recalibrated for every experiment. To avoid a drift, all samples from one experiment were measured without interruption. However, a certain drift of the values cannot be excluded because the measurements took several hours; we estimate the error at up to 10%. In the experiments with combined tracers (^{18}O, iodide, Br, and BB), Br was measured by ion chromatography (Deutsche METROHM). The error in the ion chromatography is estimated at 5 to 10%. However, the samples had to be diluted 1:100 prior to the measurement, and an operator error cannot be excluded.

Basic Viscous Flow Relationships

In this contribution, VF in unsaturated permeable media generalizes the Hagen–Poiseuille approach (flow in thin tubes) to such an extent that effects of dimensions, shapes, and frequencies of active flow paths are similarly summarized as in Darcy's law of flow in saturated permeable media. Therefore, there is no need to

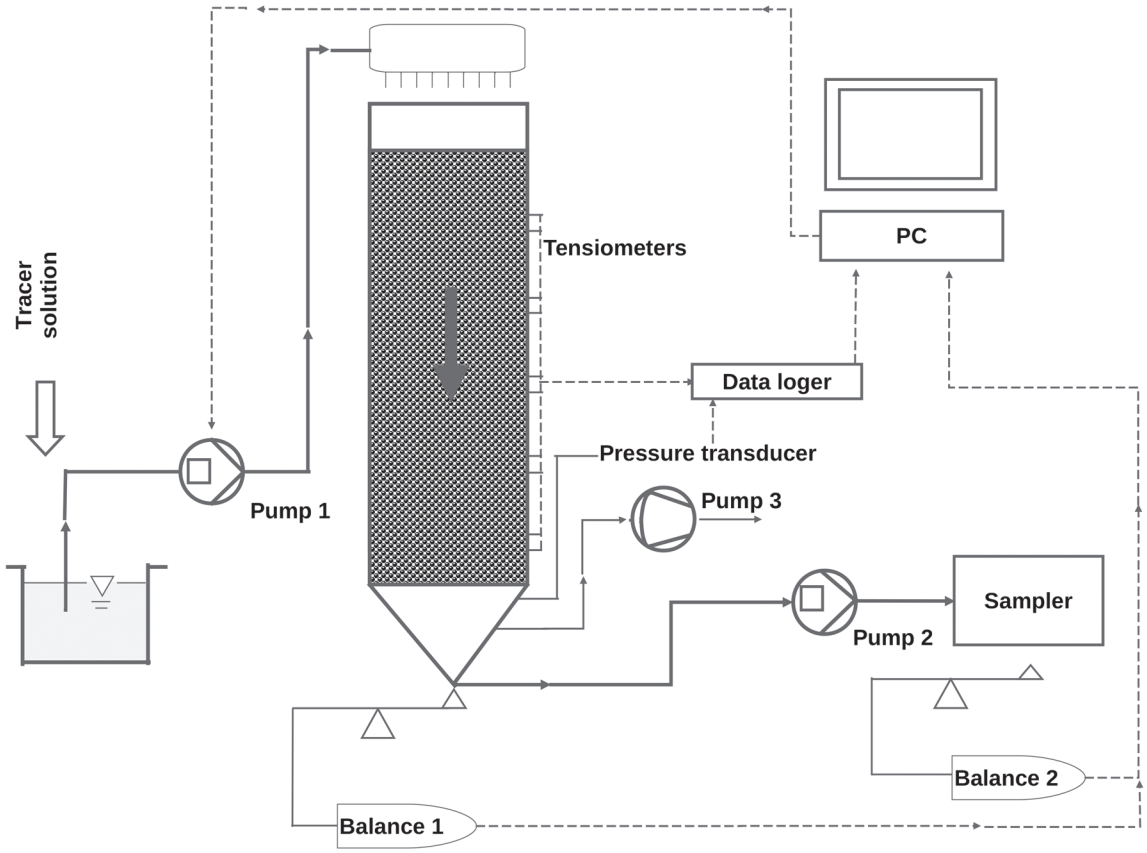

Fig. 1. Schematic representation of the experimental setup.

a priori assume properties of those paths; quite the contrary, VF with the two parameters film thickness F and specific contact area L adequately describes the processes of infiltration and drainage, whereas the two parameters follow from an a posteriori analysis. Germann (2018a) presented the VF approach in great detail.

The VF approach (Germann, 2014, 2018a) to infiltration in partially saturated permeable media is based on three frequently observed prerequisites:

1. The sharp wetting front (e.g., Selker et al., 1992) indicates a discontinuity between the already wetted volume from the shock front to the surface of the medium, and the unaffected volume of the permeable medium bellow the front.
2. The constant velocity v of the wetting shock front (e.g., Selker et al., 1992; Germann and al Hagrey, 2008) expresses the balance between accelerating and decelerating forces, hence momentum balance during flow.
3. The collapse to atmospheric pressure of capillary potential behind the wetting front (e.g., Germann and al Hagrey, 2008; Nimmo, 2012; Germann, 2018b) demonstrates that the infiltrating water short-circuits the capillary forces.

Newton's (1729) law of shear takes care of Prerequisites 1 and 2, whereas the consequences of Prerequisite 3 follow further down. The concept of gravity-driven flow in partially saturated permeable media relies on a cohesive water film running down (Fig. 2).

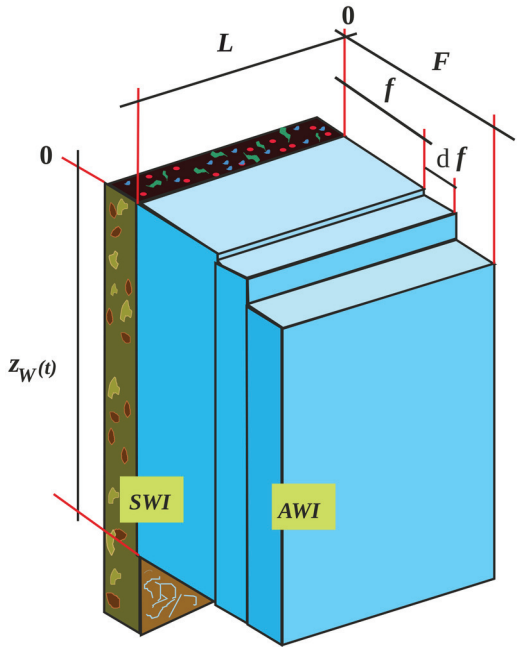

Fig. 2. Film flow along a vertical plane. F, film thickness (m); f, thickness variable (m); df, thickness of a lamina (m); $z_W(t)$, vertical position of the wetting shock front (m); L, specific contact area between the moving water film and the resting parts of the permeable medium, namely the air–water interface (AWI) and the solid–water interface (SWI) (Germann, 2014, with permission).

A rectangular pulse $P(q_S,T_B,T_E)$ of water input is applied to the horizontal surface of a permeable medium, where q_S (m s^{-1}) is the volume flux density, and T_B and T_E (s) are the beginning and ending of the pulse, respectively. The $P(q_S,T_B,T_E)$ initiates at the surface the propagation of a water content wave WCW that envelops a film with thickness F (μm) and specific contact area L (m^2 m^{-3}) per cross-sectional area A (m) of the permeable medium (Fig. 2). The film is confined between the surface, the solid–water interface SWI, the air–water interface AWI, and the increasing depth of the wetting shock front at z_W (t) that represents a discontinuity. The specific contact area per volume of the medium onto which momentum dissipates amounts to $[L \times z_W(t) \times A]/[z_W(t) \times A] = L$ (m^2 m^{-3}).

The mobile water content (m^3 m^{-3}) of the WCW amounts to

$$w(z,t) = F(z,t)L \quad [1]$$

where z (m, positive down from the surface) and t (s) are the depth and time coordinates, respectively. The mobile water content w is usually inferior to the total water content θ (m^3 m^{-3}) of the permeable medium. The wetting shock front of the WCW moves with the velocity (m s^{-1})

$$v = \left(\frac{g}{3\eta}\right)F^2 \quad [2]$$

where g (= 9.81 m s^{-2}) is acceleration due to gravity and η (≈ 10^{-6} m^2 s^{-1}) is the kinematic viscosity of water. The temporal position of the WCW's wetting shock front amounts to

$$z_W(t) = v(t - T_B) = \left(\frac{g}{3\eta}\right)F^2(t - T_B) \quad [3]$$

The volume flux density within the film is

$$q(z,t) = vw(z,t) = F(z,t)^3 L\left(\frac{g}{3\eta}\right) = w(z,t)^3 \frac{g}{3\eta L^2} \quad [4]$$

The mobile water content snaps back to 0 when input ceases at T_E and a draining front starts moving with the celerity

$$c = \frac{dq}{dw} = F^2\left(\frac{g}{\eta}\right) = 3v \quad [5]$$

If input to the surface lasts long enough the wetting and draining fronts arrive at the particular depth Z (m) at times (s)

$$t_W(Z) = T_B + \frac{Z}{v} = T_B + \frac{3Z}{c} \quad [6]$$

and

$$t_D(Z) = T_E + \frac{Z}{c} \quad [7]$$

After the draining front arrival at Z, the volume flux density of drainage (m s^{-1}) recedes according to

$$q(Z,t) = q_S\left[\frac{t_D(Z) - T_E}{t - T_E}\right]^{3/2} \quad [8]$$

Given a long enough infiltration period (T_E – T_B), the following expressions apply to the depth Z (m), for instance at the bottom of our soil columns, where T_D and T_W replace the depth-dependent variables t_D (Z) and t_W (Z). Thus, according to the VF approach, the drainage flow is

$$q(Z,t) = \begin{cases} 0 & T_B \le t \le T_W \\ q_S & T_W \le t \le T_D \\ q_S\left(\dfrac{T_D - T_E}{t - T_E}\right)^{3/2} & T_D \le t \le \infty \end{cases} \quad [9]$$

From Eq. [7] follows

$$c = \frac{Z}{T_D - T_E} \quad [10]$$

Equation [5] yields the film thickness as

$$F = \sqrt{c\left(\frac{\eta}{g}\right)} \quad [11]$$

while Eq. [4] and [5] produce the mobile water content:

$$w = \frac{3q}{c} \quad [12]$$

Finally, the specific contact area follows from Eq. [1] and [11] as

$$L = \frac{w}{F} \quad [13]$$

Alluding to Eq. [1], one VF pore volume amounts to

$$V^P_{visc} = wZ = FLZ \quad [14]$$

The time required for turning over one unit of V^P_{visc} is

$$T^P_{visc} = \frac{V^P_{visc}}{q_S} \quad [15]$$

while the number of V^P_{visc} turned over during tracer delay is

$$N^P_{visc} = \frac{T_{Br}}{T^P_{visc}} \quad [16]$$

where T_{Br} is the arrival time of the Br tracer (see below for its calculation).

The VF approach relies on the parameters F and L that are determined a posteriori from time series of drainage flow. It is worth noting that no inferences are required regarding the sizes, geometries, or distributions of pores, cracks, fissures, and pipes. From Prerequisite 3 (flow under atmospheric pressure) follows that the widths of flow paths have to exceed F; otherwise, positive pressures will build up that lead to perching water at the hydromechanical scale. Germann and Prasuhn (2018), for example, analyzed drainage flow from a temporarily saturated soil at the bottom of a weighing lysimeter. At the hydrodynamical scale of pores and grains, there must be numerous spots of saturation and pressures greater than atmospheric during infiltration. However,

the conditions at these spots presumably exist only for short distances and durations because pure pressure waves move at the speed of sound in the range of 370 m s^{-1} (Blum et al., 2004), whereas distances to the next flow paths of adequate widths might be in the range of millimeters. Thus, equilibration to atmospheric pressure in nonsaturated permeable media may occur within 10^{-3} to 10^{-2} s.

Data Pretreatment and Estimation of Viscous Flow Parameters

The original time series of drainage weights were noisy because bottles from the autosampler had to be changed manually. Therefore, we removed erroneous values, aggregated the data by calculating the median per 30 s, and smoothed them by locally weighted regression (LOESS, degree = 2, span = 0.05; Cleveland and Devlin, 1988). Because the LOESS smoother would also smooth the edges of the drainage curve and thus affect the estimation of the VF parameters (see below), we only smoothed the data during the steady-state flow.

From the experimental protocol follow $q(Z, t)$, $T_B = 0$, and T_E (end of irrigation). The arrival time of either the wetting front T_W or the draining front T_D is the only unknown parameter to be matched when interpreting drainage with the VF framework. The value of T_D is determined by fitting Eq. [8] to the drainage data by minimizing the sum of squared residuals to the observed drainage flow. Finally, T_W is calculated by combining Eq. [6] and [7] as

$$T_W = T_B + 3(T_D - T_E) \quad [17]$$

Relationships between Bromide Delay and Viscous Flow Parameters

We elucidated the relationships of the delay Δ_{Br} (s) of Br breakthrough with the basic VF parameters thickness F and specific contact area L of the water film. The arrival time of Br, T_{Br} (s), is set equal to the time of the first noticeable concentration increase. To estimate T_{Br}, we first smoothed the time series of Br concentrations in the drainage solution with a LOESS smoother (degree = 2, span = 0.2). Subsequently, we determined T_{Br} as the maximum curvature of the smoothed curve in the interval where on visual inspection the Br concentration started to rise. The curvature is defined as $|d_2/(1 + d_1^2)^{3/2}|$, with d_1 and d_2 being the first and the second derivatives of the Br concentrations in the drainage. The manual restriction to a certain time interval only was necessary because the concentrations varied in the beginning of experiments, in particular when soil columns where already subjected to an irrigation with Br (i.e., for irrigation rates >10 mm h^{-1}). Bromide delay Δ_{Br} is defined as the time difference between the observed beginning of the drainage (i.e., when water starts to drain from the soil column) $T_{W,obs}$ and T_{Br}.

We analyzed the correlations of Δ_{Br} delays with the two VF parameters F and L, and their combinations F (proportional to velocity v, Eq. [2]), $F \times L$ (proportional to the mobile water content of w, Eq. [1]), $F^2 \times L$ (proportional to $v \times L$, Eq. [1] and [2]), and $F^3 \times L$ (proportional to the flux q_S, Eq. [4]). Because we did not assume linear correlations between Δ_{Br} and the VF parameters, we calculated the rank-based Spearman correlation coefficient ρ. To determine its significance, we used permutation tests that are nonparametric (i.e., no assumption made about the shape of data distribution) and that are suitable for small datasets (Sidak et al., 1999). In a permutation test, the available data are permuted many times to determine the p value.

Additionally, we ranked the different VF parameters according to their importance in predicting Δ_{Br}. As a prediction model, we used random forests (RF), which is based on an ensemble of regression trees and can handle correlated predictors (Breiman, 2001). For every decision tree, a new bootstrap sample of the training data is created and the tree is fitted to the data. Thus, for every single regression tree, the data not selected in the bootstrap sample to train the model can be used to test it. The average mean squared error (MSE) for every data point across the whole ensemble of regression trees is reported as the so called out-of-bag error. Unlike a linear model, RF can be used for nonlinear relationships. It has three parameters, namely, the number of variables sampled randomly at each tree node from the set of possible variables (mtry, default is 1/3 × the number of predictors), the minimal size of the terminal nodes (nodesize, default is 5 for regression), and the number of trees in the forest (ntree). According to the advice by Kuhn and Johnson (2013), we set ntree = 1000 and kept the other parameters at their default values (mtry = 2 in our case) because RF is robust against overfitting (Strobl et al., 2009). The strength of the association of a predictor with the response (i.e., its importance) in RF is assessed by a so-called "variable importance" based on permutation. A predictor is randomly permuted and the difference of the MSE to the unpermuted case is computed. If the MSE increases substantially, then the predictor is important and strongly associated with the response (Breiman, 2001).

Results

Comparison between Tracers and the Influence of Suction and Repacking

The breakthrough of Br and ^{18}O in the experiments without suction and irrigation rate of 64 mm h^{-1} occurred concurrently (Fig. 3). Except in the experiment with C3, the breakthrough curves of the two tracers were comparable. Thus, no retardation of Br compared with ^{18}O was recorded, and we can consider Br as a conservative tracer. The last four values of the normalized Br concentration c/c_0 in C3 exceed 1.0 and are probably due to a measurement or dilution error.

Because two experiments per column were performed with the irrigation intensity of 64 mm h^{-1} with and without suction at the bottom, respectively, we can compare the influence of suction on the Br breakthrough (Fig. 4; Table 1). Although the suction reduced T_{Br} in columns C1 and C4, it had hardly any effect in C2 and C3. Note that different final levels of Br concentrations in columns C2 and C4 are due to an early stop of irrigation (see above).

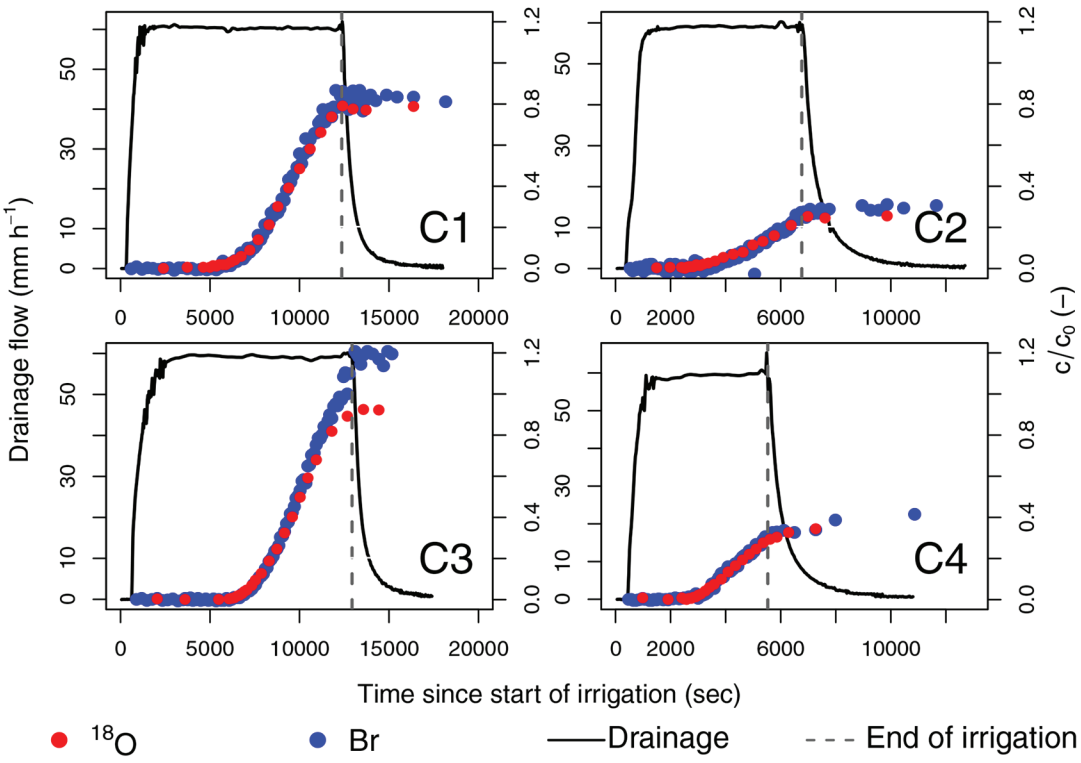

Fig. 3. Breakthrough curves of Br and ^{18}O in experiments with 64 mm h^{-1} without suction. The columns C1 and C3 are repacked, and columns C2 and C4 undisturbed. c/c_0, normalized concentration.

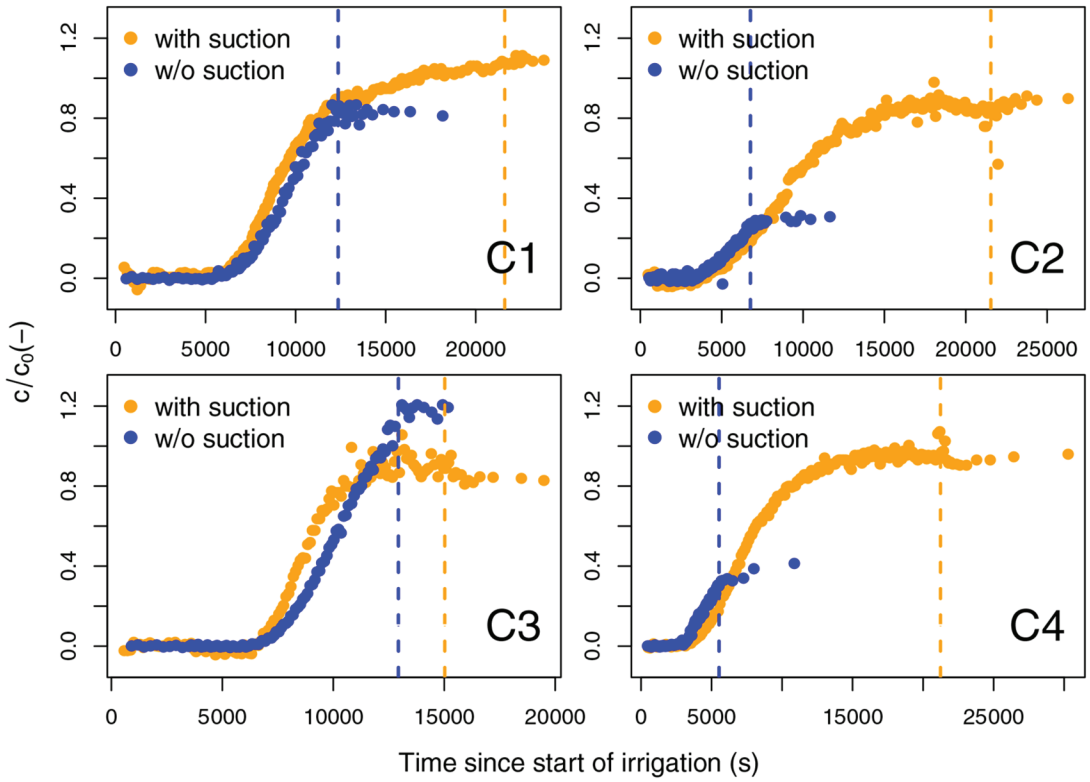

Fig. 4. Comparison of Br breakthrough at 64 mm h^{-1} with and without suction at the bottom of the columns. The columns C1 and C3 are repacked, and columns C2 and C4 undisturbed. The dashed lines indicate the end of irrigation (blue = without suction and orange = with suction). c/c_0, normalized concentration.

Table 1. Viscous flow characteristics and arrival of the Br tracer.

Column	Characteristic†									
	q_S	T_E	$T_{W,obs}$	T_W	T_D	T_{Br}	Δ_{Br}	F	L	N^p_{visc}
	10^{-6} m s^{-1}	s						μm	m^{-1}	
C1 (repacked)	2.79	64,410	1,230	1,260	64,830	37,169	35,939	8.5	1,374.7	29.5
	9.18	34,140	210	810	34,410	10,100	9,890	10.6	2,328.3	12.5
	16.65	21,630	210	630	21,840	6,011	5,801	12.1	2,897.4	9.5
	16.73‡	12,390	330	630	12,600	6,142	5,812	12.1	2,911.5	9.7
C2 (undisturbed)	2.59	72,900	60	1,980	73,560	25,826	25,766	6.8	2,515.5	13.0
	8.31	37,020	90	1,350	37,470	9,250	9,160	8.2	4,533.9	6.9
	15.80	21,540	60	900	21,840	3,458	3,398	10.1	4,694.0	3.8
	16.44‡	6,780	90	720	7,020	3,489	3,399	11.3	3,494.9	4.8
C3 (repacked)§	3.12	74,070	60	NA	NA	41,795	41,735	NA	NA	NA
	8.26	31,440	150	1,170	31,830	11,029	10,879	8.9	3,636.2	9.4
	16.53	15,030	240	810	15,300	6,418	6,178	10.6	4,193.3	7.9
	16.50‡	12,960	360	630	13,170	6,491	6,131	12.1	2,871.1	10.3
C4 (undisturbed)	2.61	79,290	60	1,800	79,890	28,389	28,329	7.1	2,191.8	15.8
	8.20	34,650	150	1,260	35,070	9,886	9,736	8.5	4,038.1	7.8
	16.66	21,240	60	810	21,510	3,150	3,090	10.6	4,227.9	3.9
	16.68‡	5,550	270	630	5,760	3,168	2,898	12.1	2,902.4	5.0

† q_S is the steady volume flux density of infiltration and drainage calculated from the drainage data; T_E is the end of infiltration (beginning of the pulse [T_B] = 0); $T_{W,obs}$ and T_W are the observed and calculated arrival times of wetting front, respectively; T_D is the arrival time of the draining front as estimated from the optimized Eq.[8] to the data; T_{Br} is the time of first noticeable increase of Br concentration; $\Delta_{Br} = T_{Br} - T_{W,obs}$; F is the film thickness; L is the specific contact area; and N^p_{visc} is the number of viscous flow volumes turned over.
‡ Experiments without suction at the bottom of the column.
§ Data from column C3, 10 mm h^{-1}, are excluded from further analyses. NA, not available.

The two repacked soil columns were considered to demonstrate the difference of macroporosity vis-à-vis the undisturbed columns. The film thickness F can be thought of as the narrowest path taken by the mobile water during infiltration. As Table 1 indicates, the repacked column C1 shows slightly thicker films than its undisturbed counterpart C2, whereas hardly any difference occurs between C3 and C4. The specific contact area L, however, shows marked differences between C1 and C2 in that repacking has substantially reduced L. The same effect occurs in C3 when comparing L values with C4, yet to a much smaller extent than in C1 and C2.

Viscous Flow Parameters and Bromide Delay

The data used to estimate the VF parameters are shown in Supplemental Fig. S1. The experiment in C3 with 10 mm h^{-1} did not reach a steady state, probably due to a problem with the pump. As shown in Supplemental Fig. S1, the drainage flow increased from ~40,000 s and exceeded the nominal (programmed) irrigation rate at the end of the experiment, indicating a technical problem. Because this experiment does not fulfill the requirement of a rectangular pulse as an irrigation signal at the top of the column (see above), it was excluded from the estimation of VF parameters.

Visually, the quality of the fit of Eq. [8] to the drainage data increased when q_S was estimated from the data (as the average flow between $0.9T_E$ and T_E) instead of using the nominal programmed irrigation rate. However, the differences between both flow rates were small (Supplemental Fig. S2). The film thickness F ranged between 6.8 and 12.1 μm and the specific contact area L between 1374.7 and 4694.0 m^{-1}, respectively (Table 1). In general, F and L both increased with increasing irrigation rate. However, for experiments at 64 mm h^{-1} without suction, F was larger and L smaller compared with experiments with suction at the same irrigation rate (Supplemental Fig. S4).

The observed beginning of drainage $T_{W,obs}$ was significantly lower by 285 s in experiments with undisturbed columns (bootstrap 95% confidence intervals: [723.6, 113.0]). Drainage started particularly late in C1 during the first experiment ($q_S = 2.79 \times 10^{-6}$ m s^{-1}). This might be due to a smaller antecedent water content because the weight of C1 was roughly 100 g less than at the beginning of the subsequent experiments. By contrast, although the mean of T_{Br} in repacked columns is larger than in undisturbed, the difference is not significant, probably because of the large spread of the values and a small sample.

The T_{Br} decreased with increasing q_S (Supplemental Fig. S5). There was no clear relationship between the observed beginning of the drainage $T_{W,obs}$ and the tracer breakthrough time T_{Br}. However, the latter was clearly correlated with the calculated arrival of the wetting front T_W (Fig. 5). The T_W was calculated

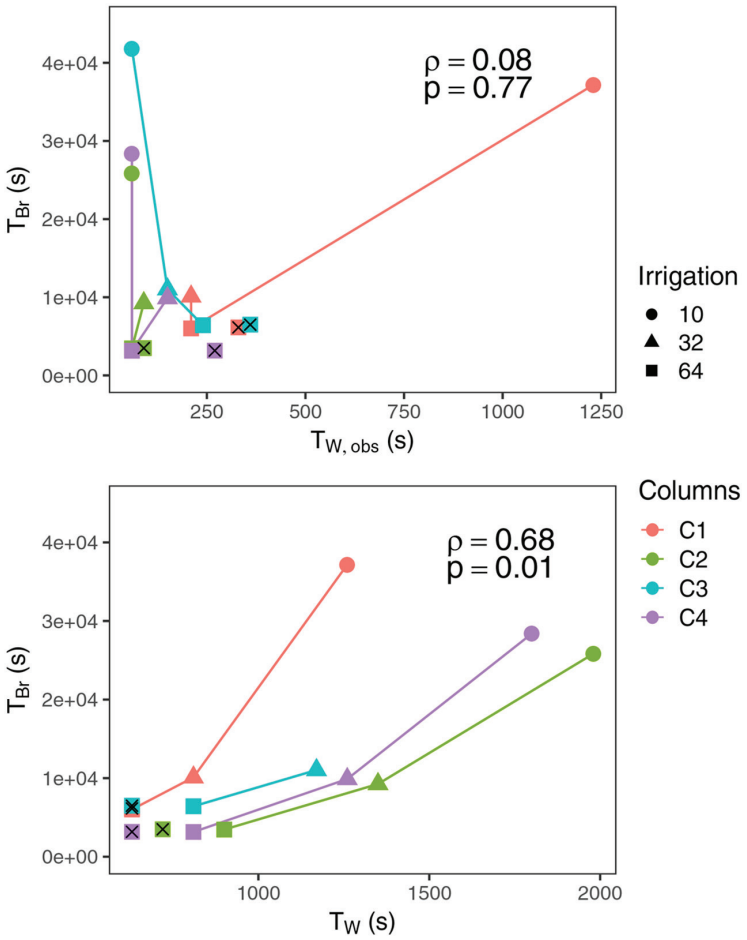

Fig. 5. Relationship between T_{Br} (the arrival time of Br), the observed beginning of the drainage, and the calculated arrival of the drainage front T_w. Irrigation rates are in mm h^{-1} and experiments without suction at the bottom of the columns are marked with ×.

back from the arrival time T_D of the draining front (Eq. [6] and [7]), whereas T_D followed from matching Eq. [8] to the data of the receding tail of $q(Z, t > T_D)$. The receding tails of the drainage curves follow the VF expectation more closely than the arrivals of the wetting shock fronts T_W. The latter represent sharp discontinuities in theory (Eq. [2]); however, in reality, they experience local disturbances presumably at the lower boundary of the columns.

The Δ_{Br} was negatively correlated with the VF parameters ($\rho \in [-0.55, -0.89]$) (Fig. 6). All correlations were significant. The largest correlation was calculated to $L \times F$, $L \times F^3$, and $L \times F^2$. The RF model explained 81% of variance in the data and confirmed the stronger association between Δ_{Br} and these combinations of VF parameters by a larger variable importance (Fig. 7). The RF model is known to suffer from a bias when calculating variable importance for correlated predictors. Thus, we compared the calculation of variable importance (Fig. 7) with a conditional variant suggested by Strobl et al. (2008) and obtained the same grouping; namely, $L \times F$, $L \times F^2$, and $L \times F^3$ are the most important predictors for Δ_{Br}.

Discussion

The comparison of Br with ^{18}O breakthrough (Fig. 3) categorizes Br as a conservative tracer. The delay of Br breakthrough, Δ_{Br}, with respect to the observed arrival $T_{W, obs}$ of the wetting shock front at the bottom of the soil columns was related to the VF parameters film thickness F and specific contact area L, and to their combinations. As Fig. 6 and 7 reveal, the correlations between Δ_{Br} and VF parameters increases from L, F, and F^2 ($\rho \in [-0.55, -0.71]$), to $L \times$ F, $L \times F^3$, and on to $L \times F^2$ ($\rho \in [-0.83, -0.89]$). Although the correlations with F and L are significant, their combinations explain the delay better and deserve closer inspection. The $L \times$ F combination ($\rho = -0.83$) represents the mobile water content w during steady flow (Eq. [1]); however, it merely combines spatial flow properties. The $L \times F^3$ combination ($\rho = -0.83$) is proportional to the rate of preferential flow q_S as the product of w and the velocity v of the wetting shock front (Eq. [4]). Thus, this combination includes aspects of the tracer's residence time. The outstanding combination of $L \times F^2$ ($\rho = -0.89$) embraces F^2 that is proportional to v relating to the tracer's residence time, and to L representing the surface area available for fast tracer exchange with the stagnant antecedent (i.e., "old") water. Because $\rho < 0$, Δ_{Br} decreases as $L \times F^2$ increases (i.e., the faster the water film moves and the wider the contact area between mobile and stagnant water becomes, the shorter is the delay of tracer breakthrough). Increasing F is presumably related to longer diffusion paths that would increase Δ_{Br}. However, the correlation between Δ_{Br} and F equals −0.71, and thus the length of diffusion paths in and out of the water film is of less concern in this study, where F varies from 6.8 to 12.1 μm. In cases with wider variations of F, diffusion path lengths might be significant to the delay of tracer breakthrough. The number of turned over VF volumes N^P_{visc} (Eq. [16]) ranges from 3.8 to 29.5 (Table 1). Particularly, the N^P_{visc} values in experiments with smaller irrigation rates (10 and 32 mm h^{-1}) are disturbingly large, to which we cannot offer a reasonable explanation at the present.

The VF approach deals with the exchange of Br as conservative tracer from the mobile water in preferential flow with the sessile parts of the soil. Maxima of film thickness F and specific contact area L were in the ranges of 12 μm and 5000 m^{-1}, respectively, representing the undisclosed arrangements and geometries of the flow paths that are lined with undisclosed proportions of solids and water. Both, thin F and huge L may explain rapid tracer exchange from the mobile water into the sessile parts as the statistical analyses have revealed. We consider these results as a solid point of departure for future experiments.

The comparison between the performances of undisturbed vs. repacked soil columns is weakly conclusive. Most prominent is the reduction of the specific contact area L due to the repacking of column C1. Thus, in our study, the effect of repacking of soil on flow and tracer transport is primarily the reduction of connectivity

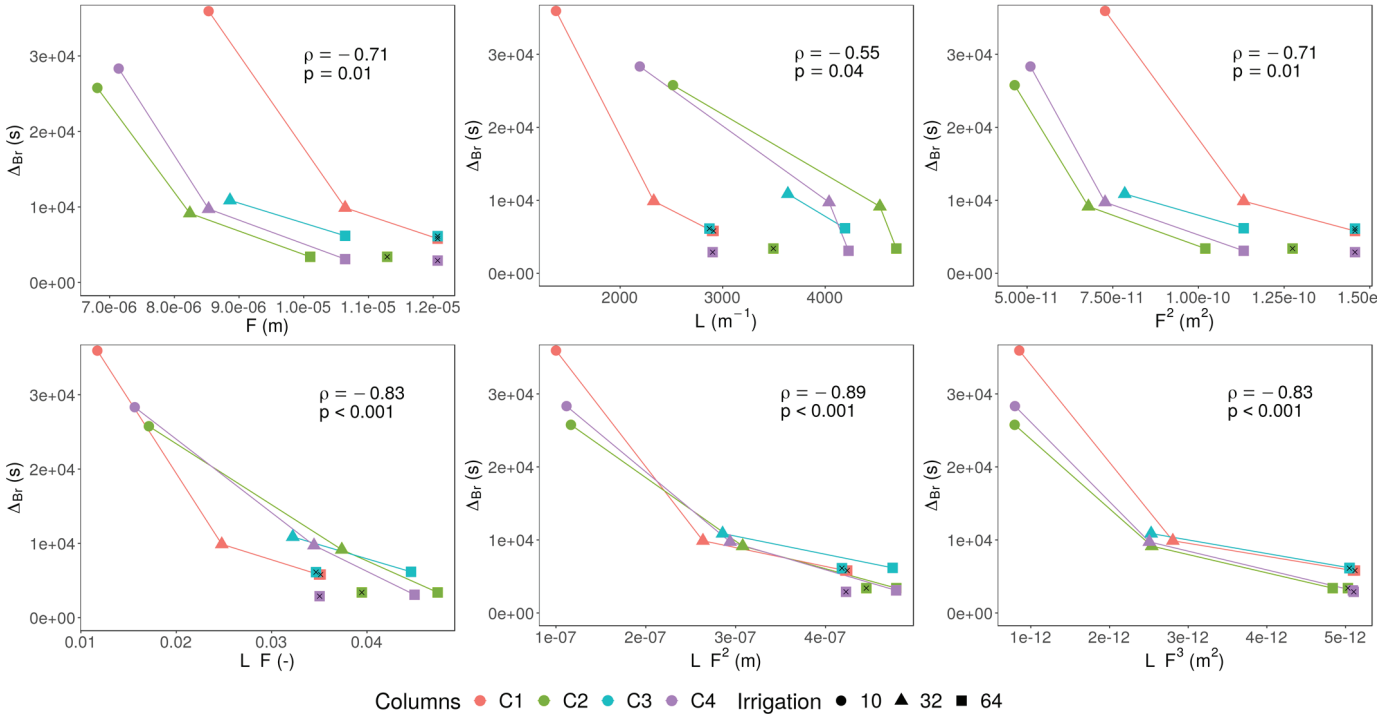

Fig. 6. Relationships between Δ_{Br} (i.e., time difference between the observed beginning of the drainage and the arrival time of Br [T_{Br}]) and different combinations of viscous flow parameters. The *p* values are based on a permutation test of Spearman's ρ. Irrigation rates are in mm h^{-1} and experiments without suction at the bottom of the columns are marked with a cross. *F*, film thickness (m); *L*, specific contact area between the moving water film and the resting parts of the permeable medium.

among flow paths in the range of 5 to 15 μm and not the removal of macropores in the range of 300 to 500 μm (Jarvis et al., 2016).

With the exception of C1, the suction applied to the bottom of soil columns affects mainly *L* (Table 1). The specific contact area increases prominently with suction, indicating that the artificial condition at the lower boundary exploits additional VF paths. The comparison also supports the notion that VF occurs under or close to atmospheric pressure conditions. The procedure of additional suction should be avoided in future VF investigation for the sake of comparability.

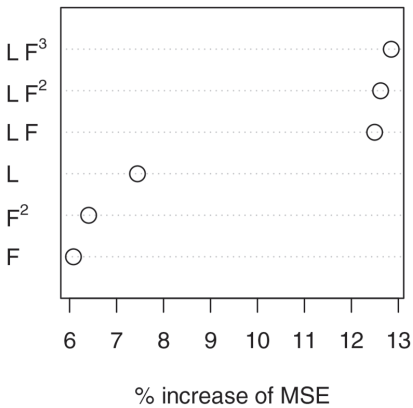

Fig. 7. Permutation variable importance in the random forests model. The combinations of the viscous flow parameters $L \times F$, $L \times F^2$, and $L \times F^3$ are the most important predictors for Δ_{Br} (i.e., time difference between the observed beginning of the drainage and the arrival time of Br [T_{Br}]). *F*, film thickness (m); *L*, specific contact area between the moving water film and the resting parts of the permeable medium; MSE, mean squared error.

Viscous flow does not require any parameter to split the porous medium in a mobile and immobile domains or a priori knowledge of pore sizes and geometries, nor does it assume a particular type of preferential flow like macropore flow, flow in cracks, or finger flow. Thus, we could successfully apply VF to undisturbed as well as repacked soil columns with possibly different pore sizes, geometries, and connectivities. Regardless of the column type (i.e., undisturbed or repacked), the tracer delay correlated strongly with VF parameters proportional to tracer's residence time, and the surface area available for fast tracer exchange. This fact calls for a shift in focus from studying macropore flow as a separate and distinct flow phenomenon to a more unifying study of hydromechanical foundations of infiltration. In particular, our results emphasize that preferential flow and the process of POOW are related phenomena and should be studied together. The transport of tracers can be accelerated or retarded through exchange between "new" and "old" water—a process worth investigating given possible implications for ground water contamination, for example. Viscous flow provides a unifying framework to study both preferential flow and POOW as long as the flow is laminar (i.e., the film thickness *F* lies between ∼2 and 120 μm) and the pressure is roughly atmospheric.

Conclusions

The VF approach provides a coherent hydromechanical framework for the experimental investigation of POOW at the scale of soil columns and soil profiles. To avoid boundary effects as they may occur in soil columns or lysimeters (Germann and al Hagrey, 2008; Germann and Prasuhn, 2018), the approach should be applied to infiltration of conservative tracers at the profile scale. Water and solute sensors—for instance, salt-sensitive time domain reflectometry (TDR) probes—are capable of rapidly monitoring water contents and tracer concentrations in situ with high enough resolutions suited for POOW research under conditions closer to reality. The large numbers of mobile water turnovers N^{P}_{visc} before bromide breakthrough awaits in-depth research that may gain support from similar tracer studies in lysimeters.

In soil hydrology, most approaches to preferential flow conventionally adhere to some minor or major degree to flow and transport in soil macropores as, for instance, Beven and Germann (1982) have put forward and as Jarvis et al. (2016) have summarized. The VF approach to the delay of bromide breakthrough, and thus the POOW process, suggest that the exchange of tracer occurs even faster than fast preferential flow advance. In catchment hydrology, better understanding POOW is a necessary stepping stone in the development of the promising velocity–celerity concepts as, for instance, McDonnell and Beven (2014) have debated.

Supplemental Material

The supplemental material contains figures showing the drainage flow and the relative concentration of Br in all 16 breakthrough experiments, the differences between the nominal and the estimated volume flux density, the comparison of the measured and the modeled drainage flow, the variation of F and L with the estimated volume flux density, and the decrease of T_{Br} with the estimated volume flux density. Additionally, tables with information on properties of the studied soils and the summary of irrigation experiments can be consulted.

Acknowledgments

We thank Gisela Wiedemann, who performed the tracer experiments as part of her diploma thesis, and Prof. Dr. Bernd Huwe for fruitful discussions and support during the project. The Department of Hydrology (University of Bayreuth) is acknowledge for the measurements of Br by ion chromatography. This study was supported by the German Research Foundation (DFG FOR 562, Grant no. Hu-636/11-1).

References

Atallah, N., and M. Abou Najm. 2019. Characterization of synthetic porous media using non-Newtonian fluids: Experimental evidence. Eur. J. Soil Sci. 70:257–267. doi:10.1111/ejss.12746

Beven, K., and P. Germann. 1982. Macropores and water flow in soils. Water Resour. Res. 18:1311–1325. doi:10.1029/WR018i005p01311

Beven, K. 2018. A century of denial: Preferential and nonequilibrium water flow in soils, 1864–1984. Vadose Zone J. 17:180153. doi:10.2136/vzj2018.08.0153

Blum A, I. Flammer, T. Friedli, and P. Germann. 2004. Acoustic tomography applied to water flow in unsaturated soils. Vadose Zone J. 3:288–299. doi:10.2136/vzj2004.2880

Bogner, C. 2009. Analysis of flow patterns and flow mechanisms in soils. Ph.D. diss. Univ. of Bayreuth, Bayreuth, Germany.

Breiman, L. 2001. Random forests. Mach. Learn. 45:5–32. doi:10.1023/A:1010933404324

Cleveland, W.S., and S.J. Devlin. 1988. Locally weighted regression: An approach to regression analysis by local fitting. J. Am. Stat. Assoc. 83:596–610. doi:10.1080/01621459.1988.10478639

Gerke, H.H., P. Germann, and J. Nieber. 2010. Preferential and unstable flow: From the pore to the catchment scale. Vadose Zone J. 9:207–212. doi:10.2136/vzj2010.0059

Germann, P. 2014. Preferential flow: Stokes approach to infiltration and drainage. Geographica Bernensia, Univ. of Bern. https://boris.unibe.ch/119081/1/preferential_flow.pdf (accessed 25 July 2019).

Germann, P. 2018a. Preferential flow at the Darcy scale: Parameters from water content time series. Methods Soil Anal. 3:160121. doi:10.2136/msa2016.0121

Germann, P.F. 2018b. Viscosity: The weak link between Darcy's law and Richards' capillary flow. Hydrol. Processes 32:1166–1172. doi:10.1002/hyp.11450

Germann, P.F., and S.A. al Hagrey. 2008. Gravity-driven and viscosity-dominated infiltration into a full-scale sand model. Vadose Zone J. 7:1160–1169. doi:10.2136/vzj2007.0172

Germann, P.F., and M. Karlen. 2016. Viscous-flow approach to in situ infiltration and in vitro saturated hydraulic conductivity determination. Vadose Zone J. 15(2). doi:10.2136/vzj2015.05.0065

Germann, P.F., and V. Prasuhn. 2018. Viscous flow approach to rapid infiltration and drainage in a weighing lysimeter. Vadose Zone J. 17:170020. doi:10.2136/vzj2017.01.0020

Jarvis, N., J. Koestel, and M. Larsbo. 2016. Understanding preferential flow in the vadose zone: Recent advances and future prospects. Vadose Zone J. 15(12). doi:10.2136/vzj2016.09.0075

Kirchner, J.W. 2003. A double paradox in catchment hydrology and geochemistry. Hydrol. Processes 17:871–874. doi:10.1002/hyp.5108

Kuhn, M., and K. Johnson. 2013. Applied predictive modeling. Springer, New York. doi:10.1007/978-1-4614-6849-3

McDonnell, J.J., and K. Beven. 2014. Debates—the future of hydrological sciences: A (common) path forward? A call to action aimed at understanding velocities, celerities and residence time distributions of the headwater hydrograph. Water Resour. Res. 50:5342–5350. doi:10.1002/2013WR015141

Newton, I. 1729. The mathematical principles of natural philosophy: Translation into English. Vol. II. Benjamin Motte, London.

Nimmo, J.R. 2010. Theory for source-responsive and free-surface film modeling of unsaturated flow. Vadose Zone J. 9:295–306. doi:10.2136/vzj2009.0085

Nimmo, J.R. 2012. Preferential flow occurs in unsaturated conditions. Hydrol. Processes 26:786–789. doi:10.1002/hyp.8380

Selker, J., J.Y. Parlange, and T. Steenhuis. 1992. Fingered flow in two dimensions: 2. Predicting finger moisture profile. Water Resour. Res. 28:2523–2528. doi:10.1029/92WR00962

Šidák, Z., P.K. Sen, and J. Hájek. 1999. Theory of rank tests. 2nd ed. Academic Press, San Diego.

Strobl, C., A.L. Boulesteix, T. Kneib, T. Augustin, and A. Zeileis. 2008. Conditional variable importance for random forests. BMC Bioinformatics 9:307. doi:10.1186/1471-2105-9-307

Strobl, C., J. Malley, and G. Tutz. 2009. An introduction to recursive partitioning: Rationale, application, and characteristics of classification and regression trees, bagging, and random forests. Psychol. Methods 14:323–348. doi:10.1037/a0016973

Tetzlaff, D., C. Birkel, J. Dick, J. Geris, and C. Soulsby. 2014. Storage dynamics in hydropedological units control hillslope connectivity, runoff generation, and the evolution of catchment transit time distributions. Water Resour. Res. 50:969–985. doi:10.1002/2013WR014147

von Freyberg, J., B. Studer, M. Rinderer, and J.W. Kirchner. 2018. Studying catchment storm response using event and pre-event water volumes as fractions of precipitation rather than discharge. Hydrol. Earth Syst. Sci.22:5847–5865. doi:10.5194/hess-2018-401